

A scalable platform for biomechanical studies of tissue cutting forces

This article has been downloaded from IOPscience. Please scroll down to see the full text article.

2009 Meas. Sci. Technol. 20 045801

(<http://iopscience.iop.org/0957-0233/20/4/045801>)

The Table of Contents and more related content is available

Download details:

IP Address: 193.205.81.13

The article was downloaded on 20/02/2009 at 08:17

Please note that terms and conditions apply.

A scalable platform for biomechanical studies of tissue cutting forces

P Valdastri¹, S Tognarelli¹, A Menciassi^{1,2} and P Dario^{1,2}

¹ CRIM Lab, Scuola Superiore Sant'Anna, Pontedera, Italy

² Italian Institute of Technology Network, Genova, Italy

E-mail: valdastri@sssup.it

Received 16 November 2008, in final form 23 December 2008

Published 19 February 2009

Online at stacks.iop.org/MST/20/045801

Abstract

This paper presents a novel and scalable experimental platform for biomechanical analysis of tissue cutting that exploits a triaxial force-sensitive scalpel and a high resolution vision system. Real-time measurements of cutting forces can be used simultaneously with accurate visual information in order to extract important biomechanical clues in real time that would aid the surgeon during minimally invasive intervention in preserving healthy tissues. Furthermore, the *in vivo* data gathered can be used for modeling the viscoelastic behavior of soft tissues, which is an important issue in surgical simulator development. Thanks to a modular approach, this platform can be scaled down, thus enabling *in vivo* real-time robotic applications. Several cutting experiments were conducted with soft porcine tissues (lung, liver and kidney) chosen as ideal candidates for biopsy procedures. The cutting force curves show repeated self-similar units of localized loading followed by unloading. With regards to tissue properties, the depth of cut plays a significant role in the magnitude of the cutting force acting on the blade. Image processing techniques and dedicated algorithms were used to outline the surface of the tissues and estimate the time variation of the depth of cut. The depth of cut was finally used to obtain the normalized cutting force, thus allowing comparative biomechanical analysis.

Keywords: soft tissue cutting, MEMS sensor, triaxial forces, tissue biomechanics, MIS

(Some figures in this article are in colour only in the electronic version)

1. Introduction

Measuring the mechanical response of a soft biological tissue during cutting in minimally invasive surgical (MIS) procedures would pave the way for a dramatic reduction of operative trauma and hospitalization time. Despite MIS having been used for more than 25 years [1], it still brings severe limitations to the surgeon. Difficult hand-eye coordination, reduced depth perception and haptic limitations represent the most important problems for the medical user. Usually, a surgeon wants to feel forces [2], positions and tactile information generated by the instruments in order to avoid any possible tissue damage. However, the current surgical procedures lack reliable feedback related to interaction forces between the instruments and the surrounding environment. Besides, histological evidence shows that excessive forces applied to tissues may obstruct the blood supply and lead to localized

necrosis [3]. Accordingly, the role of force sensing in the interaction between a surgical instrument and the patient's tissues is essential for accurate medical performances. If the surgical instrument is a scalpel, reliable information about mechanical interactions of the blade with the patient's organs would aid the surgeon in minimizing the regional tissue distortion and destruction, obtaining better wound healing and better scar once the incision is closed by either external staples or subcutaneous sutures. Thus, thanks to the acquisition of interaction forces, real improvement of a surgeon's performances can be achieved from a clinical standpoint. Furthermore, real-time measurements of cutting forces can be used simultaneously with accurate visual information. In particular, having a measure of the blade penetration depth during cutting would enable to bias the signal against the natural bulge in the thickness direction presented by biological tissues during cutting. This is fundamental

information in order to extract significant biomechanical clues that would aid the surgeon in preserving healthy tissues [4]. Nevertheless, biomechanical tissue responses can be used in modeling the tissue properties by an *in vivo* data set. Nowadays, there is growing interest in tissue analysis in order to perform surgical planning, diagnosis and training, yet until now it has been very difficult to acquire realistic data [5–8]. Therefore, modeling the response of several deformable soft tissues during cutting procedures becomes fundamental for developing more realistic surgical simulators [9].

In order to achieve this goal, the combined use of a reliable force sensor and a real-time vision system, mechanically constrained in a stable configuration, is required. In the last few years, several robotic endoluminal platforms have been introduced in the literature for minimally invasive laparoscopy [10–12] or for natural orifice transluminal surgery (NOTES) [13]. This novel technique, relying on transluminal access, starts with a perforation of a lumen in order to reach the targeted organ by natural orifices, thus avoiding external incisions. A miniaturized robot having a surgical biopsy tool and a vision system has been described in [14]. A modular and reconfigurable robotic platform for endoluminal gastric surgery has been presented in [15, 16]. This is composed of eight joint active modules, three dedicated to surgical tasks (one camera module and two interventional modules) and a central element. In case one of the interventional modules is a force-sensitive scalpel, it can enable precise biomechanical measurements together with a camera placed on a second arm of the robotic platform. Reliable visual and force measurements would allow the robotic platform to run in an autonomous force-controlled mode, helping to prevent unintentional damage of tissue or to compensate for organ motion in the case of contact between the instrument and organ. Interaction forces could be displayed back to the surgeon, providing him/her with direct information of the stresses applied to the organ during cutting. This can be obtained, for example, with augmented reality (AR) [17] by displaying visual information related to the force in the form of bars, contours or contour surfaces, superimposed on real-time camera images.

A uniaxial force sensor can be used to determine if a device has contacted the environment and to control or limit the contact force. However, a force is completely known as far as all its three components are measured. Thus, for a fully dextrous robotic device, it is desirable to acquire forces on all three axes. Interesting examples of three-dimensional force sensors placed on the tip of surgical instruments are reported in [18] for a grasper and in [19] for a scalpel. In these solutions, the technology used for sensing consists of traditional metallic structures with commercial strain gauges, and therefore these systems are difficult to be further scaled in dimensions.

Another relevant issue to consider is that the closer to the interaction point the force is sensed the more the information is relevant to give real feedback about the contact. However, in several examples reported in the literature [20–22], the force is acquired at the external end of the instrument, so that the measured contact forces are distorted through the shaft. On the other hand, placing the sensor on the instrument tip is more

challenging from a technological viewpoint, since it must be miniaturized and the connecting cables must be adequately packaged to run inside the device [5, 23].

A suitable solution for triaxial force sensing which overcomes all the above-mentioned open issues has been reported in [24]. It consists of a silicon microelectromechanical system (MEMS) based piezoresistive triaxial force sensor [25] integrated into a cutting tool for MIS. The main efforts of that work were devoted to increase the robustness of the silicon transducer through proper packaging, in order to enable its use in surgical applications. The overloading limits for the bare MEMS are 3 N for normal loadings and 0.5 N for tangential loadings [26]. In order to increase these limits, a compliant polyurethane filling was selected to embed the force sensor. Furthermore, a nylon sphere was used as a mechanical interface between the blade and the polyurethane filling to transmit the force to the sensor in a symmetrical way, so that information about the stimulus orientation was maintained. Despite the successful integration into a miniaturized surgical device, this system was not optimized in terms of sensitivity, signal bandwidth and robustness.

The goal of this work is to present a complete platform for real-time biomechanical analysis of biological tissue cutting that can be scaled down in size and used in endoluminal or transgastric robotic procedures. This platform takes advantage of an improved design of the triaxial-sensitive cutting tool described in [24] used together with a real-time video image recorder. Both these systems can be miniaturized in order to enable MIS operations, provided a rigid link is maintained between the tool and the camera. Further details about scalability will be provided later in the paper. The same platform can also be used to obtain *in vivo* data sets for haptic modeling of tissue properties, as proposed in [7, 9, 27, 28].

The paper is organized as follows. A description of the sensor design and fabrication is given in section 2. In the same section, an overview of the vision module and the related algorithm for edge detection is also reported. The device calibration is described in section 3. *Ex vivo* cutting experiments on several different tissues are reported in section 4, while conclusions and future works are illustrated in section 5.

2. System design and fabrication

2.1. Sensor design

In a previous version of the sensing device [24], a nylon ball was selected and a sharp ruby blade was glued to the flat surface of the nylon ball. Even if the results obtained with this solution were encouraging, the mechanical bonding between the nylon ball and the polyurethane filling was not optimal and ball detachment was observed for tangential forces having a module larger than 3 N. Also, the glue bonding between the ruby blade and the nylon ball was shown to be unreliable for high lateral forces applied to the blade, especially for loadings oriented perpendicularly to their main lateral dimension. For this reason, a surgical blade was shaped as in figure 1 by

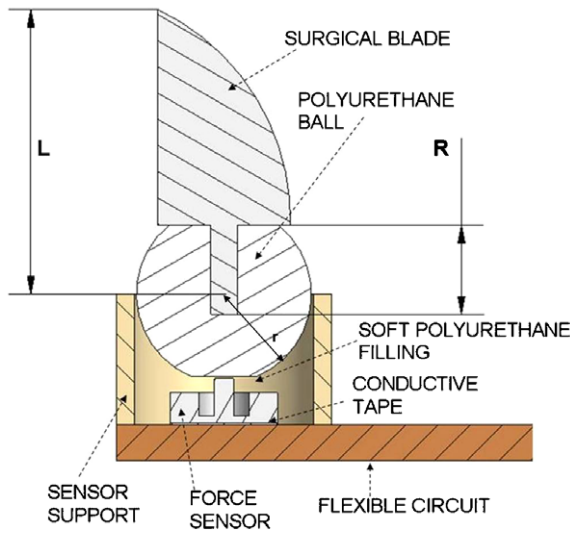
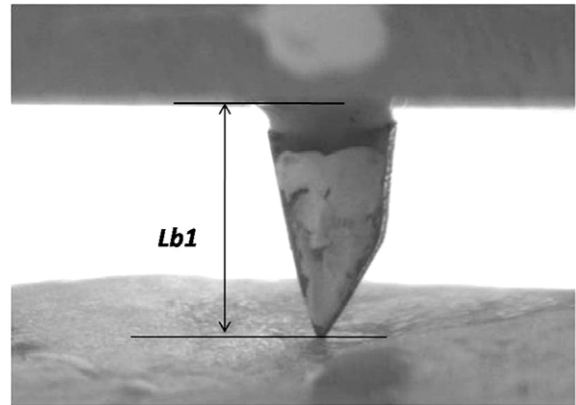


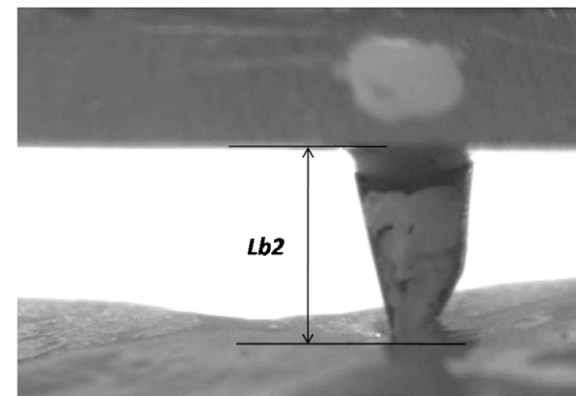
Figure 1. Cross-section of the sensing device.

μ wire EDM (AP 200 L, Sodick, Japan), leaving a 1.25 mm long ‘root’ (R in figure 1) on the opposite side of the blade tip. A hard polyurethane ball was then polymerized around the ‘root’ of the blade. In this way, a relevant improvement in the mechanical bonding between the blade and the spherical element was achieved. Better performances in terms of lateral peak forces were also guaranteed by the mechanical properties of the chemical bonding between the soft polyurethane filling and the hard polyurethane of the spherical element.

The side of the polymeric ball facing the sensor was polished with sand paper in order to obtain a flat surface. In this case, compared with the original round shape of the ball, compressive stresses were allowed to be spread over a larger surface, thus increasing the efficiency of force transmission. As regards tangential loadings, in the case of a round shape, the force transmission from the ball to the bare sensor was obtained by the effect of ball rotation on the soft polyurethane layer between the ball and the top of the sensing column of the silicon device. Having a flat bottom allowed the ball to push laterally a higher amount of soft polyurethane, thus also exerting a lateral pressure on the column of the bare silicon



(A)



(B)

Figure 3. Snapshots from the camera for the depth of cut estimation using image processing. In (A) the blade is totally outside the tissue, while in (B) it is penetrating the tissue for a depth of $L_{b1} - L_{b2}$.

sensor. The bottom side of the sphere was placed almost in contact with the silicon force sensor, thus maximizing force transmission and minimizing hysteresis due to the viscoelastic behavior of the polymer. The polyurethane filling, penetrating inside the MEMS sensor cavities, prevented failures of the silicon chip.

The polyurethane ball has a diameter of 2.5 mm and the length L , as shown in figure 1, is 3.7 mm. The outer diameter of the final device is 2.95 mm.

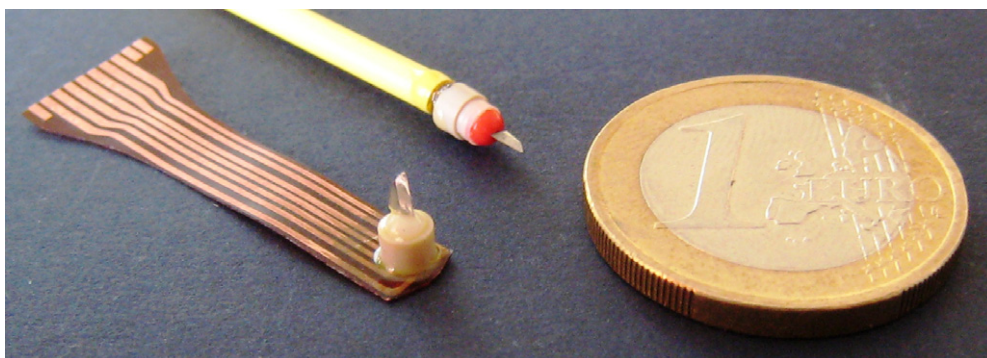


Figure 2. A sensing device with a cross-shaped flexible circuit is integrated into a 9 French catheter (upper part). In the lower part of the picture, a sensing device with a flat-shaped flexible circuit is represented.

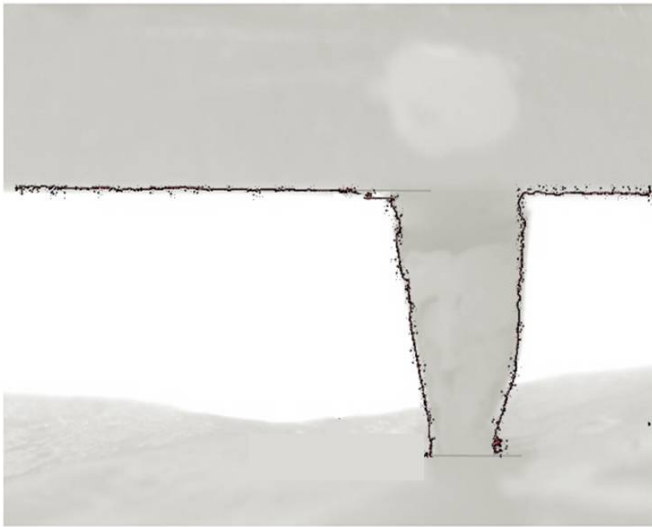


Figure 4. Edge detection superimposed on the corresponding camera snapshot.

A cross-shaped design for the flexible circuit enabled the wiring of electrical signals through the lumen of a 9 French catheter as represented in the upper side of figure 2. Proper electronic circuitry allows us to convert the fractional changes in the resistance of the piezoresistors into measurable voltages.

2.2. Sensor fabrication

The improvements applied to the procedure described in [24] were mainly related to the ball–blade assembly. The first step of fabrication was to mechanically and electrically connect the silicon sensor to a custom-shaped flexible circuit, obtained from LF9150R Pyralux (DuPont, USA), by using the Z-Axis Conductive Film 5552R (3M, USA) as described in [29]. Then the sensor support (fabricated in polyether ether ketone (PEEKTM), by using a five-axis CNC machining center) was glued onto the flexible circuit using a UV-light curing adhesive (ELC 4481, Electro-Lite, USA). The glue was dispensed on four single spots in order to leave free spaces between the copper tracks of the flexible circuit and the lower edge of the PEEK cylinder. These spaces allowed the excess of the soft polyurethane to flow out during one of the following steps of the assembly procedure. Before gluing, the inner surface of

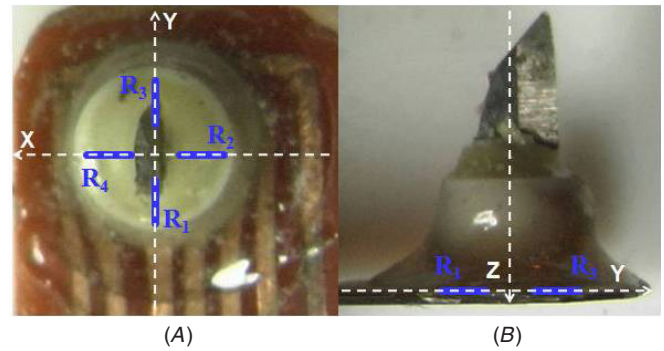


Figure 6. Adopted Cartesian reference system, superimposed on a top (A) and a lateral (B) view of the cutting device.

the support was polished with a fine file in order to improve the adhesion of the polymeric filling.

A silicon mould was obtained by pouring silicon (Silastic 3481, Silgard) all around a 2.5 mm diameter nylon ball, where a shaped surgical blade was previously inserted by sticking the ‘root’ into a drilled hole. This mould was then used to polymerize hard polyurethane (PC26, Camattini spa, Italy) around the ‘root’ of a shaped surgical blade. Then, a thickness of 0.1 mm was removed from the bottom of the ball in order to obtain a flat side as in figure 1.

In the next step, 10 mg of soft polyurethane (Poly 74-45, PolyTek, USA) was dispensed into the housing and evacuated in a vacuum oven, to avoid the presence of air bubbles in the material. Then, the hard polyurethane ball, having the surgical blade embedded in it, was inserted with the flat side facing the top of the force sensor. This step was performed before the complete polymerization of the soft polyurethane. The ball was pushed down as much as possible and the excess of the soft polymer was able to flow out through the spaces between the copper tracks and the lower edge of the PEEK cylinder.

After a curing time of 24 h, the final device was ready to be used. Two possible configurations are represented in figure 2. These are different in the shape of the flexible circuit. The one in the bottom part of the picture has a flat-shaped circuit and can be easily plugged into an electronic system by using a standard connector for flexible circuits. The other device takes advantage of a cross-shaped flexible circuit, thus enabling its integration into a 9 French surgical instrument, such as a multi-lumen catheter.

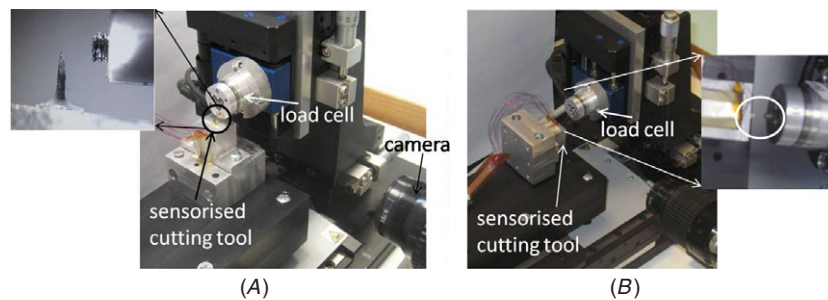


Figure 5. Calibration test bench during normal and tangential loading conditions.

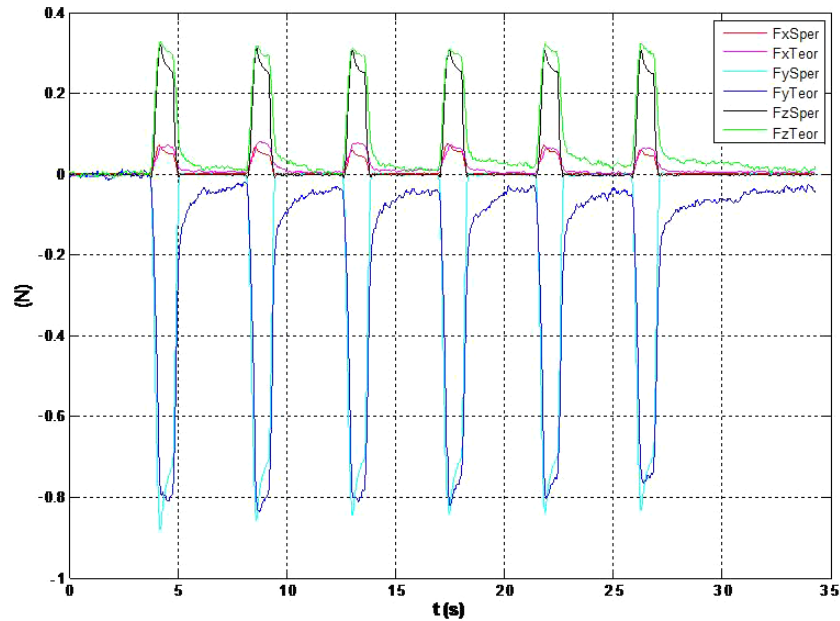


Figure 7. Comparison between the signal acquired by the reference load cell (F_x Sper, F_y Sper and F_z Sper) and the forces reconstructed from the sensor by applying the calibration matrix (F_x Teor, F_y Teor and F_z Teor).

2.3. Vision system

The depth of cut plays a significant role in the recorded cutting force. This value usually increases during cutting because of the natural bulge in the thickness direction of soft biological tissues, thus affecting the cutting force exerted by the blade [9]. Therefore, having an apparatus that can measure the penetration depth of the blade in the tissue would allow us to normalize the cutting forces with the depth of cut, thus obtaining relevant biomechanical clues that can be used for comparative analysis.

In order to achieve this goal, an ultracompact black and white camera (uEye UI-2250-M, iDS, Germany) with a Universal Serial Bus (USB) 2.0 interface was used. This camera is provided with 1/1.8" SONY charge coupled device (CCD) sensors with 1600×1200 pixel resolution and a maximum of 12 frames per second (fps). A circular mount coupler (1-6010, Navitar, Rochester, NY) with an additional dedicated adapter (0.5 \times adapter 1-60439, Navitar, Rochester, NY) was mounted onto the camera. Besides, in order to complete the optical system, zoom lens (Zoom 5.5 \times w/12 mm F.F 1-60135D, Navitar, Rochester, NY) and lens attachment (1-60111-0.75 \times , Navitar, Rochester, NY) were assembled on the camera equipment. This vision module was used to capture the cutting video during the whole procedure at 4 fps, and all the images were analyzed offline by using the image processing toolbox of Matlab 7.5.0 (MathWorks, USA).

As the video was acquired, split-level postprocessing was performed. An edge detection algorithm, implemented by a dedicated Simulink (Matlab 7.5.0, MathWorks, USA) model, and a purposely developed Matlab 7.5 routine were used to outline the surface of the tissue in the imaging window and to estimate the distance from the blade support to the edge of the tissue top surface, as represented in figure 3. The depth of cut, which corresponds to the blade portion inside the tissue,

was calculated as the difference between the total blade length (L_{b1}) and the instantaneous exposed blade side (L_{b2}):

$$\text{Depth}(y) = L_{b1} - L_{b2}(y). \quad (1)$$

In the experimental setup, the total blade length L_{b1} is 3.6 mm, while L_{b2} changes as the cutting progressed.

An example of tissue surface and blade edge detection processing techniques are shown in figure 4.

It is relevant to outline that all the implemented image processing can also run in real time by lowering the resolution of the video stream, thus reducing the processing burden. Therefore, if the system is scaled down for endoluminal surgery applications, information coming from the vision module can be processed in real time together with force signals, in order to obtain biomechanical information that can improve surgical performances during operation. Commercially available cameras³ can be used for a scaled version of the proposed platform.

3. Sensor calibration

The force sensor was calibrated with the same system used in [24]. It consisted of a six-component load cell (ATI NANO 17 F/T, Apex, NC), mechanically connected to a servo-controlled nanotranslator (M-111DG, PI, Karlsruhe, Germany), having a travel range of 15 mm and a movement resolution of 7 nm. The slider applies a controlled load to the blade, as represented in figure 5.

Three different loading tests, one normal and two tangential (the tangential ones are along the x - and y -axis directions, defined in figure 6), were performed in order to obtain the sensor calibration matrix K . In particular, the setup

³ Medigus Ltd Israel URL <http://www.medigus.com>.

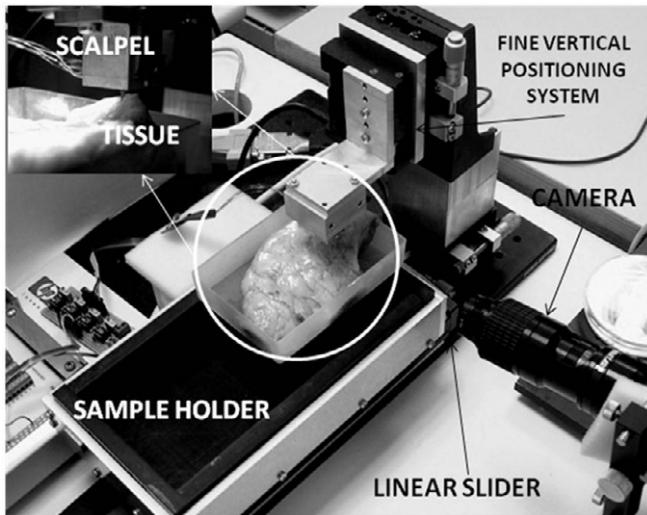


Figure 8. Global view of the experimental setup. Inset: zoom of the scalpel during a tissue cutting test.

represented in figure 5(A) was used during tangential tests and the sensor was rotated 90° along the z -axis switching from X to Y trials. For normal loadings, the load cell was pushed on the tip of the blade, loading and unloading it along the z -direction, as represented in figure 5(B). The calibration matrix can be applied to directly evaluate the real-time force (vector \bar{F}) from the four values of fractional changes in resistance (vector $\frac{\Delta R}{R}$) by applying

$$\bar{F} = K \frac{\Delta R}{R}. \quad (2)$$

For the calibration procedure, the servo-controlled nanoslider was programmed to apply ten loading–unloading cycles. The span was dependent on the axis under test. During normal loading, a force increasing from 0 N up to 10 N was applied along the z -direction at a translational constant speed of 1.4 mm s⁻¹. For the calibration tests along x - and y -directions, the loading span was from 0 N up to 2 N at the same velocity. The forces recorded by the load cell during the loading cycle along the y -axis are plotted in figure 7 as F_x Sper, F_y Sper and F_z Sper.

The K matrix for the proposed device resulted:

$$K = \begin{pmatrix} 13 & 19 & 54 & -67 \\ 149 & -130 & 26 & -6 \\ -110 & -11 & -25 & -185 \end{pmatrix} \text{N}, \quad (3)$$

and the experimental sensitivity matrix S_E , which is the Moore–Penrose pseudoinverse of matrix K , was

$$S_E = \begin{pmatrix} 39 & 28 & -23 \\ 67 & -46 & -30 \\ 102 & -7 & -28 \\ -41 & -13 & -35 \end{pmatrix} \times 10^{-4} \text{N}^{-1}. \quad (4)$$

Thus the sensitivities, defined as in [26], were

$$S_x = 102 \times 10^{-4} \text{N}^{-1}$$

$$S_y = 46 \times 10^{-4} \text{N}^{-1}$$

$$S_z = 30 \times 10^{-4} \text{N}^{-1}.$$

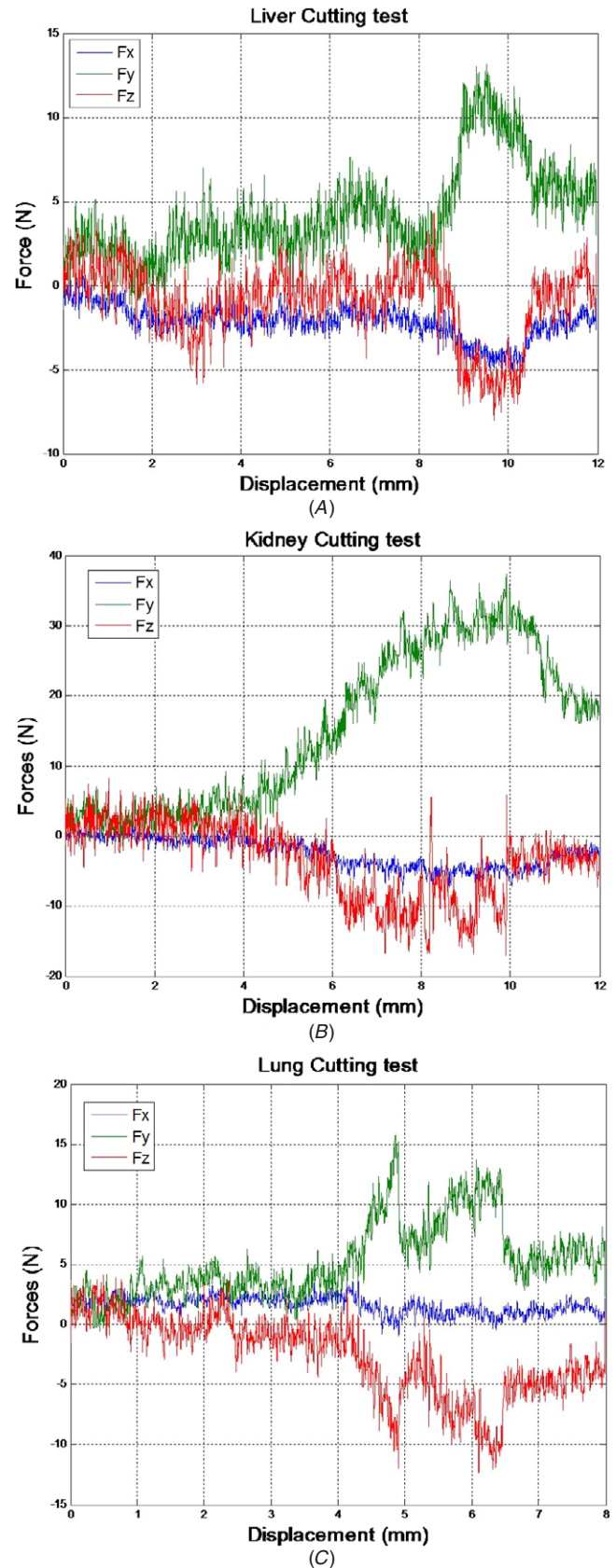


Figure 9. Sensor outputs during cutting tests on different porcine tissues: (A) liver, (B) kidney, (C) lung.

Thanks to the new and optimized sensor design, these values are more than one order of magnitude higher than that of the sensor reported in [24].

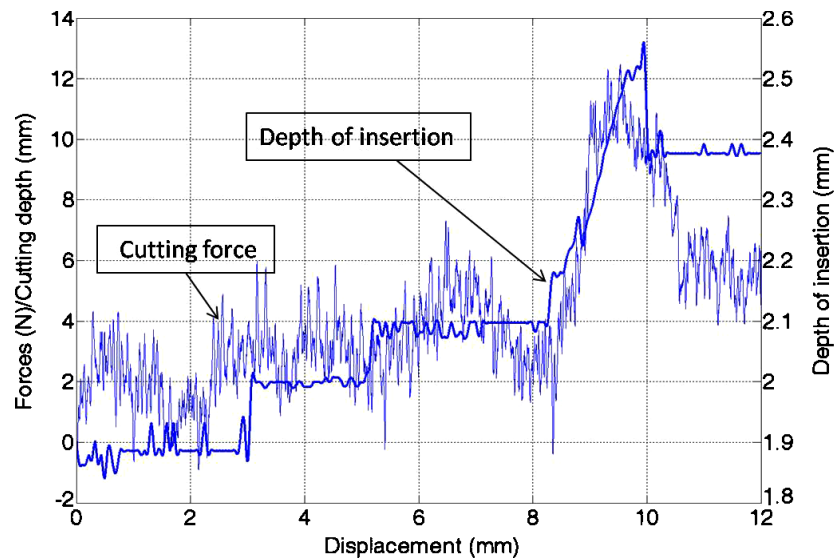


Figure 10. Force recorded in the y -direction and depth of penetration during the liver cutting test.

The results obtained by applying equation (2) with the obtained K matrix are reported in figure 7 as F_x Teor, F_y Teor and F_z Teor for a loading–unloading cycle along the y -axis, corresponding to the cutting direction of the scalpel.

Thanks to the improvement in the sensor design, the bandwidth of the current device is 500 Hz, thus covering all the relevant frequencies for haptic feedback and tissue mechanical properties measurement (i.e. from dc to hundreds of Hz [30]). Also, the maximum loading forces improved in the novel design. Regarding normal loading, it was 50 N, while for pure tangential forces a plastic deformation of the polymeric structure occurred at 3 N. In order to prevent this situation, a cap with a slot for the blade can be designed in order to stop the lateral blade movement before the critical threshold is reached.

The normal force resolution was about 50 mN for the unfiltered signal. Considering a force range between 0 N and 50 N, the resolution in terms of bits was 9.2. As regards tangential forces, the unfiltered resolution was 40 mN, thus 7.6 bits over a range that spanned from -3 N to 3 N. These performances can be improved by applying low-pass filtering, once the bandwidth of the force signal is known.

4. In vitro validation for tissue analysis

In order to validate the capabilities of the proposed platform in supplying reliable biomechanical data for soft tissue cutting procedures, a set of experiments were performed on different biological tissues. In particular, freshly harvested samples of porcine liver, kidney and lung were chosen because they are the most likely targets for robot-assisted surgical procedures [31].

4.1. Experimental setup description

The experimental test bench used in this work is illustrated in figure 8. The sensor was mounted into the same support used for calibration and connected to a proper electronic interface

for data acquisition. The whole subsystem was placed onto a servo-controlled translator (M-111DG, PI, Karlsruhe, Germany), allowing fine position tuning in the vertical direction. Rough placement of the sensor was enabled by three micrometric translation stages with crossed roller bearing (M-105.10, PI, Karlsruhe, Germany). The tissue sample holder was mounted on a servo-controlled linear stage (M-410CG, PI, Karlsruhe, Germany). The maximum stroke of the slider is 100 mm, with an adjustable speed of up to 1 mm s^{-1} . A proportional derivative (PD) controller was implemented in order to enable precise movement of the slider during cutting. The design and construction of the cutting assembly ensured that the system was sufficiently rigid and had minimal backlash, so that the forces recorded by the sensor were those obtained just by the tissue cutting action.

The tissue holder was composed of two different parts. An external metallic carrier with an internal box fabricated in Derlin was screwed to the linear stage and a plastic frame was fitted into it. The plastic inner part of the tissue holder enabled easy replacement of tissue samples. The specimens were glued with cyanoacrylate adhesive to the walls of the plastic box, in order to obtain a constrained boundary and to simulate the physiological environment of the different tissues.

The vision system described in section 2.3 was placed close to the experimental setup in order to capture both the image of the blade and the tissue profile as the cutting progressed. This information, as detailed above, allowed us to evaluate the depth of penetration of the blade as cutting occurred. A snapshot of the edge detection algorithm running is reported in figure 4.

Since the experiments were performed on *ex vivo* tissue samples, a saline solution (NaCl, 9%) was sprayed on the specimen once every 3 min in order to maintain physiological conditions and to avoid drying. The triaxial force signals were acquired by a personal computer and stored together with the slider motion information and camera files.

Regarding the experimental procedure, the vertical manual sliders were used to introduce the blade vertically into

the tissue for about 2 mm. Then a continuous translational motion was imposed on the horizontal slider in the y -direction, with a speed of 0.14 mm s^{-1} .

4.2. Results

Typical experimental triaxial force plots are represented in figure 9 for liver, kidney and lung samples. A moving average filtering with a span of ten samples was applied to the force signals in order to reduce high frequency noise. From these data, it was possible to identify the typical cutting path described in [9] as a consequence of tissue deformation and tissue fractures. In this particular cutting mode, where the blade travels almost parallel to the tissue plane, F_y can be used to give the surgeon feedback about which phase of the cutting cycle occurs.

According to the experimental results, F_y was not the only significant component of the force signal. A relevant amount of force along the vertical direction was usually present. F_z could be explained in terms of tissue accumulation. During the phase of tissue deformation, the warpage of the tissue out of plane causes a downward force due to friction on the blade. The maximum values of F_y and F_z coincide with the point of cut initiation, where tissue warping is maximum. The lateral component F_x was usually negligible, but can give interesting clues especially in fiber-oriented tissues.

Since different porcine organs were used for tests, variable amounts of average force were required in cutting procedures and the scalpel demonstrated good performances during the whole test sessions and in all the required force ranges. In particular, the liver tissue (figure 9(A)) has a maximum force drop of about 10 N due mainly to the cutting of fibers of Glisson's capsule localized around the whole organ. The highest value of force reported in figure 9, i.e. 25 N, was recorded during the cutting of a kidney sample (figure 9(B)), while the lung tissues (figure 9(C)) required an intermediate amount of incision force compared to the other two tissues. The behavior of the characteristic forces described in figure 9(B) could be related to the thick external fibrous capsule surrounding the kidney surface. The high number of alveoli and the spongy nature of the lung specimens induced a force drop of 16 N, as is visible at the end of the plot of figure 9(C).

As described above, a camera was used to analyze how deep the blade was in the specimens during cutting. The obtained values of the blade depth of cut were then used to normalize the experimentally recorded cutting forces.

Figure 10 shows the force plot for the liver sample and the relative depth of cut profile. Experimental results reveal that the cutting force and the depth of cut versus displacement exhibit similar behavior. In addition, the depth variation has the same trend as the specimens' outline.

The same forces represented in figure 9 were normalized with the experimental cutting depths, and the results are reported in figure 11. The normalization of cutting force becomes necessary in order to provide quantitative figures about tissue deformation resistance during cutting. Therefore, it was possible to compare the real forces applied to the different tissues by the blade. The same behavior that was

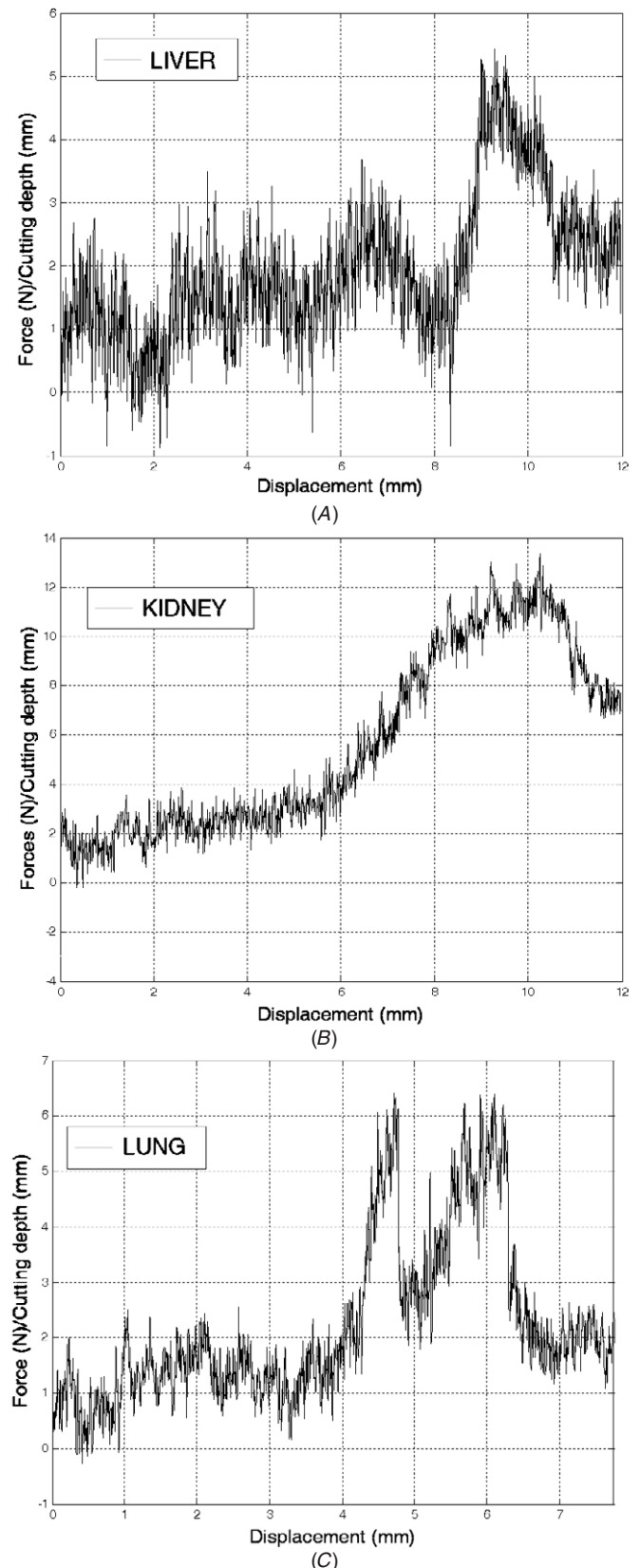


Figure 11. Normalized force in the y -direction for (A) liver, (B) kidney, (C) lung test.

described in figure 9 was also obtained in figure 11, but the maximum force values were closer, once normalized. Also in

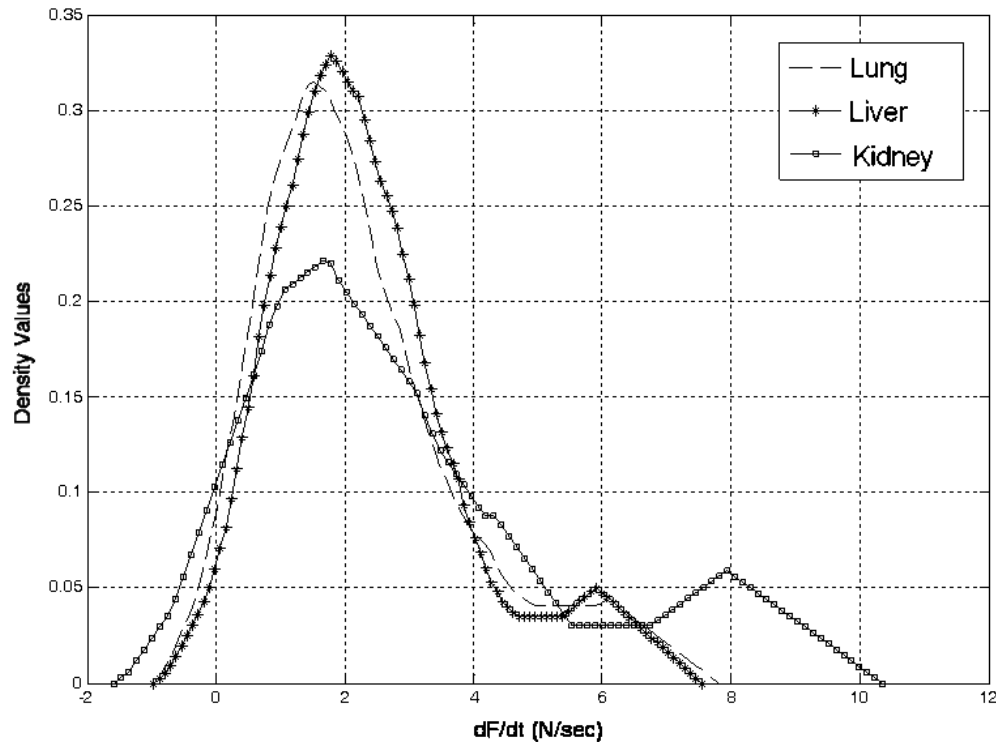


Figure 12. Statistical distribution of pseudo-stiffness for different tissues.

this case, the liver specimens required the lower cutting force and the lung tissues required the higher one. The cutting force curves obtained from the liver experiments were consistent with those reported in the literature [9], thus demonstrating the reliable performance of the platform.

As described in [9], a local parameter (local effective modulus (LEM)) can be used to measure the deformation resistance of soft tissue. The quantitative estimation of the LEM immediately before the extension phase of the cut provides an important clue for the development of consistent haptic surgical simulators. In [9], tissue resistance during the deformation phase of liver cutting procedures was estimated iteratively by means of an inverse problem with finite element models, using force measurements as the starting point. In a similar way, by means of a dedicated algorithm, it was possible to select local monotonic loading segments in the force plots. The values obtained were normalized with the time variation, corresponding to displacement since the slider was moved at a constant speed and used for statistical analysis.

The final normal statistical distribution of these characteristic coefficients are represented in figure 12 for the different tissues. It is worthy of note that these plots show narrow density curves, thus demonstrating the reliable force stability during the cutting procedures. The coefficients of the linear analysis can be considered proportional to the tissues stiffness and they can be used to evaluate the deformation parameters for the modeling of tissues.

5. Conclusion

In the present paper, a modular cutting apparatus, composed of a miniaturized cutting force sensor, a real-time vision

system and a linear stage, was designed and developed. It is able to perform microscopic scalpel cutting of different biological tissues and record both tissue cutting forces and blade penetration depth. A MEMS-based triaxial force sensor was used to develop an accurate triaxial force sensing miniaturized scalpel and several experiments were conducted on different porcine tissues, e.g. liver, kidney, lung. During the sliding motion, cutting force and blade penetration depth were recorded. Experimental results showed that the equipment was capable of reliably measuring the intrinsic cutting forces and evaluating with high accuracy the relationship between the force and the blade depth. The experimental results are also consistent with the information reported in the literature about fracture mechanical behavior for liver samples [4, 9, 32]. The three main modules of the proposed platform are the miniaturized MEMS force sensor, a real-time vision system and a linear stage to move the blade over the tissue. The small size of the force-sensitive tool (outer diameter less than 3 mm) and the availability of miniaturized cameras allow us to scale down the whole platform without impairing the overall performances, provided a rigid link is maintained between the tool and the camera. This rigid link is required to reliably measure the depth of penetration of the blade during cutting, thus enabling force normalization. The actuator which moves the cutting tool along the tissue in the presented platform is a linear stage. This can be scaled down by using a proper mechanism design and a miniaturized electromagnetic motor. A significant example for scalability of a similar platform is reported in [14], where the authors describe a bimanual robotic system equipped with a stereoscopic camera, a gripper and a cutting device. Its small dimensions enable insertion through a standard trocar for MIS. Reduced dimensions would enable

the use of the proposed technique for endoluminal robotic intervention and NOTES procedures. For example, a surgeon can use the tissue mechanical properties, obtained by means of the real-time image and force acquisition, to drive and control a robotic manipulator during the first steps of a NOTES procedure, when the access lumen is perforated to reach the target organ. In this phase, particular care is devoted to tissue cutting in order to avoid unwanted perforations. The platform, integrated into a modular robotic frame, as proposed in [16], can also be used for biopsy procedures. The different kinds of tissues selected for the cutting experiments reported were chosen in order to evaluate the real capability of the platform to provide reliable biomechanical clues in endoscopic biopsy interventions.

Finally, the results of this study can be used for an accurate biomechanical analysis of soft tissue interaction with a surgical blade to be used in realistic simulators. To achieve this goal it is necessary to develop tissue models based on accurate haptic experimental data, which should be able to quantify the local mechanical behavior of the heterogeneous tissues during cutting tests.

Acknowledgments

This work was supported by the European Commission in the framework of the ARAKNES FP7 European Project EU/IST-2008-224565. The authors would like to thank Mr Giacomo Marini for his precious work on this topic. Special thanks to Mr C Filippeschi for his continuous and invaluable help.

References

- [1] Westebring-van der Putten E P, Goossens R H M, Jakimowicz J J and Dankelman J 2008 Haptics in minimally invasive surgery—a review *Minim. Invasive Ther. Allied Technol.* **17** 3–16
- [2] Rosen J, Hannaford B, MacFarlane M P and Sinanan M N 1999 Force controlled and teleoperated endoscopic grasper for minimally invasive surgery—experimental performance evaluation *IEEE Trans. Biomed. Eng.* **46** 1212–21
- [3] Fischer G S, Akinbiyi T, Saha S, Zand J, Talamini M, Marohn M and Taylor R 2006 Ischemia and force sensing surgical instruments for augmenting available surgeon information *Proc. IEEE Biorobotics (Pisa, Italy)* pp 1030–5
- [4] Chanthasopeephan T, Desai J P and Lau A C 2003 Measuring forces in liver cutting: new equipment and experimental results *Ann. Biomed. Eng.* **31** 1372–82
- [5] Okamura A M 2004 Methods for haptic feedback in teleoperated robot-assisted surgery *Ind. Robot* **31** 499–508
- [6] Rosen J, Brown J D, De S, Sinanan M and Hannaford B 2008 Biomechanical properties of abdominal organs *in vivo* and postmortem under compression loads *J. Biomech. Eng.* **130** 1–17
- [7] Brouwer I, Ustin J, Bentley L, Sherman A, Dhruv N and Tendick F 2001 Measuring *in vivo* animal soft tissue properties for haptic modeling in surgical simulation *Stud. Health Technol. Inf.* **81** 69–74
- [8] Wang K D and Yan G Z 2009 Research on measurement and modeling of the gastro intestine's frictional characteristics *Meas. Sci. Technol.* **20** 015803
- [9] Chanthasopeephan T, Desai J P and Lau A C W 2007 Modeling soft-tissue deformation prior to cutting for surgical simulation: finite element analysis and study of cutting parameters *IEEE Trans. Biomed. Eng.* **54** 349–59
- [10] Hager G D, Okamura A M, Whitcomb L L, Taylor R H, Kazanzides P and Fichtinger G 2008 Surgical and interventional robotics—core concepts, technology, and design *IEEE Robot. Autom. Mag.* **15** 122–30
- [11] Okamura A M, Hager G D, Whitcomb L L, Taylor R H, Fichtinger G and Kazanzides P 2008 Surgical and interventional robotics—surgical cad-cam systems *IEEE Robot. Autom. Mag.* **15** 94–102
- [12] Kazanzides P, Whitcomb L L, Fichtinger G, Taylor R H, Hager G D and Okamura A M 2008 Surgical and interventional robotics—surgical assistance systems *IEEE Robot. Autom. Mag.* **15** 84–93
- [13] Lehman A C, Rentschler M E, Farritor S M and Oleynikov D 2007 The current state of miniature *in vivo* laparoscopic robotics *J. Robot. Surg.* **1** 45–7
- [14] Rentschler M, Dumpert J, Platt S, Iagnemma K, Oleynikov D and Farritor S 2007 An *in vivo* mobile robot for surgical vision and task assistance *J. Med. Devices* **1** 23–9
- [15] NgPak A, Menciassi A, Harada K, Susilo E and Dario P 2008 Design of a bending module for assembling reconfigurable endoluminal surgical system *Proc. 6th Int. Conf. on Gerontechnology (Pisa, Italy)* vol 7 p 118
- [16] Menciassi A, Valdastrì P, Harada K and Dario P 2008 Single and multiple robotic capsules for endoluminal diagnosis and surgery *Proc. IEEE Biorobotics (Scottsdale, AZ)* pp 238–43
- [17] Saha S, Burschka D, Hasser C J, Yuh D D, Akinbiyi T, Reiley C E and Okamura A M 2006 Dynamic augmented reality for sensory substitution in robot-assisted surgical systems *28th Ann. Int. Conf. of the IEEE Engineering in Medicine and Biology Society, EMBS '06* pp 567–70
- [18] Tholey G, Pillarisetti A and Desai J P 2004 On-site three dimensional force sensing capability in a laparoscopic grasper *Ind. Robot* **31** 509–18
- [19] Ortmaier T, Weiss H and Falk V 2004 Design requirements for a new robot for minimally invasive surgery *Ind. Robot* **31** 493–8
- [20] Tholey G, Hu T, Castellanos A E and Desai J P 2002 Real-time haptic feedback in laparoscopic tools for use in gastro-intestinal surgery *Proc. 5th Int. Conf. on Medical Image Computing and Computer Assisted Intervention (MICCAI'02)* pp 66–74
- [21] Tavakoli M, Patel R V and Moallem M 2003 A force reflective master-slave system for minimally invasive surgery *Proc. Intelligent Robots and Systems (IROS 2003) (27–31 Oct.)* vol 4 pp 3077–82
- [22] Krupa A, Morel G and de Mathelin M 2002 Achieving high precision laparoscopic manipulation through adaptive force control *Proc. IEEE Int. Conf. on Robotic and Automation (ICRA'02)* vol 2 pp 1864–9
- [23] Seibold U, Kübler B and Hirzinger G 2005 Prototype of instrument for minimally invasive surgery with 6-axis force sensing capability *Proc. IEEE Int. Conf. on Robotic and Automation (ICRA'05) (Barcelona, Spain)* pp 498–503
- [24] Valdastrì P, Houston K, Menciassi A, Dario P, Sieber A, Yanagihara M and Fujie M 2007 Miniaturized cutting tool with triaxial force sensing capabilities for minimally invasive surgery *J. Med. Devices* **1** 206–11
- [25] Arena A, Valvo F, Valdastrì P, Menciassi A, Carrozza M C, Beccai L, Roccella S and Dario P 2005 Design and fabrication of a hybrid silicon three-axial force sensor for biomechanical applications *Sensors Actuators A* **120** 370–82
- [26] Valdastrì P, Roccella S, Beccai L, Cattin E, Menciassi A, Carrozza M C and Dario P 2005 Characterization of a novel hybrid silicon three-axial force sensor *Sensors Actuators A* **123–124C** 249–57
- [27] Fu Y, Yuan K, Du Q and Song W 2005 Development of a virtual surgery system with a virtual scalpel *2005 IEEE Int.*

- Conf. on Information Acquisition (27 June–3 July)*
pp 5–10
- [28] Song W and Yuan K 2005 Haptic modeling for liver cutting based on fuzzy neural network *Proc. 2005 IEEE/ASME Int. Conf. on Advanced Intelligent Mechatronics* pp 1216–20
- [29] Sieber A, Valdastri P, Houston K, Menciassi A and Dario P 2007 Flip chip microassembly of a silicon triaxial force sensor on flexible substrates *Sensors Actuators A* **142** 421–8
- [30] Ottensmeyer M P and Salisbury J K 2001 *In vivo* data acquisition instrument for solid organ mechanical property measurement *Proc. 4th Int. Conf. on Medical Image Computing and Computer Assisted Intervention (MICCAI'01)* pp 975–982
- [31] Malik A, Mellinger J D, Hazey J W, Dunkin B J and MacFadyen B V 2006 Endoluminal and transluminal surgery: current status and future possibilities *Surg. Endosc.* **20** 1179–92
- [32] Lau A C, Chanthasopeephan T and Desai J P 2004 Deformation resistance in soft tissue cutting: a parametric study *Proc. 12th Int. Symp. Haptic Interfaces for Virtual Environment and Teleoperator Systems (HAPTICS'04) (Orlando, FL)* pp 323–30